Spin-Orbit Symmetries of Conduction Electrons in Silicon

Pengke Li* and Hanan Dery

Department of Electrical and Computer Engineering, University of Rochester, Rochester, New York, 14627, USA

(Received 21 March 2011; published 1 September 2011)

We derive a spin-dependent Hamiltonian that captures the symmetry of the zone edge states in silicon. We present analytical expressions of the spin-dependent states and of spin relaxation due to electron-phonon interactions in the multivalley conduction band. We find excellent agreement with experimental results. Similar to the usage of the Kane Hamiltonian in direct band-gap semiconductors, the new Hamiltonian can be used to study spin properties of electrons in silicon.

DOI: 10.1103/PhysRevLett.107.107203 PACS numbers: 85.75.−d, 71.70.Ej, 78.60.Fi

Silicon is an ideal material choice for spintronics due to its relatively long spin relaxation time and central role in semiconductor technology. These characteristics are the reason for the wide interest in recent spin injection experiments [1–4]. To date, however, modeling of basic spin properties in silicon required elaborate numerical methods [5]. Notably, the availability of transparent spin-dependent theories in direct gap semiconductors has spurred the field of semiconductor spintronics [6]. The importance of a lucid theory that accurately describes spin properties of conduction electrons in silicon with relatively simple means is thus clear.

In the first part of this Letter, we derive a Hamiltonian that captures spin properties of conduction electrons in silicon. The Hamiltonian is constructed by its invariance to the symmetry operations of the space group G_{32}^2, which describes the symmetry of the X point at the edge of the Brillouin zone [7,8]. In silicon, the X point is closer to the absolute conduction band minimum than all other high symmetry points. While $k \cdot p$ and tight-binding models have been available for many decades [9–17], spin has heretofore been ignored since spin-orbit coupling in Si is weak [18–22] and lattice inversion symmetry causes spin degeneracy. The present work is motivated by the emergence of experimental work on spin-polarized electron transport in silicon [1–4].

In the second part, this Hamiltonian is used to elucidate the nature of *intravalley* and *intervalley* spin relaxation processes in silicon due to electron-phonon interactions. Our approach unravels the underlying physics, structure, and symmetries of dominant spin-flip mechanisms. These insights cannot be shown by state-of-the art numerical studies in which only the magnitude and temperature dependence are calculated [5]. We derive analytical forms and selection rules of the dominant spin-flip matrix elements and explain the subtle distinction between spin and momentum scattering processes. Importantly, it is shown that spin relaxation due to intravalley scattering is caused by coupling of the lower and upper conduction bands (whereas intravalley momentum relaxation is governed by dilation and uniaxial deformation potentials of the lower conduction band). The accepted intravalley spin-flip matrix element derived 50 years ago by Yafet does not reveal this effect; furthermore, it was derived with only approximate spin-orbit coupling parameters and inadequate wave vector components despite correctly predicting the wave vector power law and hence its $T^{5/2}$ dependence [23]. Significant new insights regarding the structure of intervalley spin relaxation are also revealed by the theory and will be discussed in this Letter.

Figure 1(a) shows two pairs of conduction and valence bands that are pertinent to this study. Near the X point, states and energies in this subspace are found by

$$H \begin{vmatrix} \psi_{\mathbf{k},X_1} \\ \psi_{\mathbf{k},X_4} \end{vmatrix} = \begin{pmatrix} H_{cc} & H_{cv} \\ H_{vc} & H_{vv} \end{pmatrix} \begin{vmatrix} \psi_{\mathbf{k},X_1} \\ \psi_{\mathbf{k},X_4} \end{vmatrix} = E \begin{vmatrix} \psi_{\mathbf{k},X_1} \\ \psi_{\mathbf{k},X_4} \end{vmatrix}. \quad (1)$$

Throughout this Letter, the crystal wave vector ($\mathbf{k}$) is taken with respect to the X point. The upper (lower) 4-components of a state, $\psi_{\mathbf{k},X_1}$ ($\psi_{\mathbf{k},X_4}$), represent

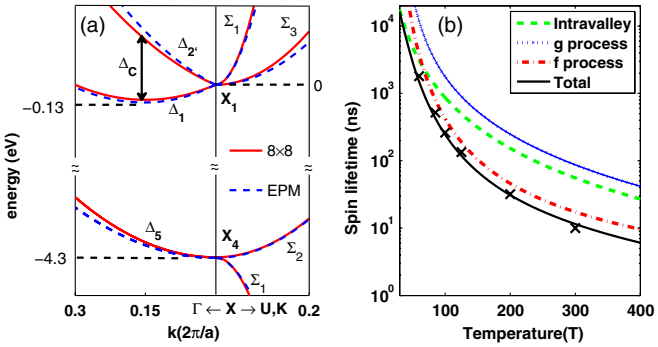

FIG. 1 (color online). (a) Calculated band structure near the X point in silicon. The wave vector origin is taken at the X point where $a = 5.43$ Å is the lattice constant. Dashed (solid) lines are results of an empirical pseudopotential model (8×8 Hamiltonian). (b) Spin relaxation in silicon due to electron-phonon interactions. Intravalley, g-process, and f-process contributions [Eqs. (13), (15), and (18)] are denoted, respectively, by the dashed green line, the dotted blue line, and the dash-dotted red line. The × symbols denote experimental results (see the text).

coefficients of the X_1 (X_4) basis functions. These basis functions belong to the X_1 (X_4) irreducible representation of G_{32}^2 [24]. H_{cc} and H_{vv} denote, respectively, conduction and valence band contributions, and $H_{cv} = H_{vc}^\dagger$ describes their coupling. These are 4×4 matrices due to the two-band and spin degeneracies at the X point of diamond crystal structures [25]. Since the energy gap at the X point, $E_{g,X} \approx 4.3$ eV, is significantly larger than other energy scales, we use Löwdin partitioning [26] and lump the valence band effect on the conduction band via

$$\begin{aligned}(H_{cc} + H_{vc}^\dagger H_{vc}/E_{g,X})|\psi_{\mathbf{k},X_1}\rangle_c &= E_\pm|\psi_{\mathbf{k},X_1}\rangle_c|\psi_{\mathbf{k},X_4}\rangle_c \\ &= (E_\pm - H_{vv})^{-1}H_{vc}|\psi_{\mathbf{k},X_1}\rangle_c \approx H_{vc}/E_{g,X}|\psi_{\mathbf{k},X_1}\rangle_c, \end{aligned} \quad (2)$$

where $\pm$ refer to the upper and lower conduction bands. The spin properties of conduction electrons are set by H_{vc}, whereas H_{vv} has a negligible effect [24]. Using the method of invariants [14], we derive H_{cc} and H_{vc} at the vicinity of the X_n point (X point along the n axis) [24]:

$$H_{cc} = \hbar^2/2m_0(k^2\mathcal{I}\otimes\mathcal{I} + 2k_0k_n\rho_z\otimes\mathcal{I}), \quad (3)$$

$$\begin{aligned}H_{vc} = &-iP(k_\ell\rho_y + ik_m\rho_z)\otimes\mathcal{I} + i\Delta_X(\rho_x\otimes\sigma_m \\ &- \mathcal{I}\otimes\sigma_\ell) + \alpha[k_n(i\rho_z\otimes\sigma_\ell - \rho_y\otimes\sigma_m) \\ &+ (ik_\ell\rho_z - k_m\rho_y)\otimes\sigma_n], \end{aligned} \quad (4)$$

where k_j denotes the jth component of the crystal wave vector with respect to the X_n point ($\{\ell, m, n\}$ is any cyclic permutation of the $\{x, y, z\}$ crystallographic axes). σ_i and $\sigma_i k_j$ components are due to spin-orbit coupling, where σ_i refer to Pauli matrices. ρ_i are invariant matrices describing the two-band degeneracy, and here we choose $\rho_i = \sigma_i$. $\mathcal{A}\otimes\mathcal{B}$ terms denote Kronecker products of 2×2 matrices. When $\mathbf{k}$ increases toward the Δ axis, the *spin-independent* basis functions of this Hamiltonian follow the compatibility relations: $X_1^1 \to \Delta_1$, $X_1^{2'} \to \Delta_2'$, $X_4^\ell \to \Delta_5^\ell$, and $X_4^m \to \Delta_5^m$ [see Fig. 1(a) for notation and Ref. [11] for details]. By using this basis, the spin-independent parameters are $\hbar k_0 = -\langle X_1^1|p_j|X_1^1\rangle = \langle X_1^{2'}|p_j|X_1^{2'}\rangle$ and $m_0P = \hbar|\langle X_1^{1,2'}|p_j|X_4^j\rangle|$, where $j = \{\ell, m\}$. In silicon, the conduction band minimum position (where thermal electrons are populated) is set by $k_0 \approx 0.15 \times 2\pi/a$, and the mass anisotropy is set by $P \approx 9$ eV · Å [11].

The model spin-dependent parameters are $\Delta_X = \lambda|\langle X_1^{1,2'}|(\nabla V \times \mathbf{p})_j|X_4^j\rangle|$ and $\alpha = \hbar\lambda|\langle X_1^{1,2'}|\nabla_j V|X_4^j\rangle|$, where $\lambda = \hbar/(4m_0^2c^2)$ and $j = \{\ell, m\}$. Using an empirical pseudopotential model [27], we estimate $\Delta_X \sim 3.5$ meV and $\alpha k_0 \sim 1.5$ meV. By substituting Eqs. (3) and (4) into Eq. (2), the upper and lower conduction bands state energies are

$$E_\pm = \frac{\hbar^2k_n^2}{2m_0} + \frac{\hbar^2(k_\ell^2 + k_m^2)}{2m_t} \pm \sqrt{E_{0,n}^2 - E_{\ell,m}^2 + |\eta|^2(k_\ell^2 + k_m^2)}. \quad (5)$$

$m_t^{-1} = m_0^{-1} + m_{cv}^{-1}$ is the transverse mass, where $m_{cv} = \hbar^2E_{g,X}/2P^2$. Other parameters are $E_{0,n} = \hbar^2k_0k_n/m_0$, $E_{\ell,m} = \hbar^2k_\ell k_m/m_{cv}$, and $\eta = 2i\Delta_X P/E_{g,X}$. Equation (5) includes only the leading spin-orbit term [24].

A crucial aspect of the model is that Eqs. (2)–(4) allow us to analytically express degenerate spin-dependent eigenstates such that $\langle\mathbf{k}, \Uparrow|\sigma_z|\mathbf{k}, \Downarrow\rangle = 0$ [23]. These eigenstates are represented by 8-component normalized vectors. The components are coefficients of the X_n-point basis functions: $\{X_1^{2'}\uparrow, X_1^{2'}\downarrow, X_1^1\uparrow, X_1^1\downarrow, X_4^\ell\uparrow, X_4^\ell\downarrow, X_4^m\uparrow, X_4^m\downarrow\}$. In the $n = z$ case (parallel to the spin quantization axis), the vectors in the *lower* conduction band read

$$\begin{aligned}|\mathbf{k}, \Uparrow\rangle \simeq \Bigg[&\frac{\sqrt{2}E_{x,y}}{\sqrt{E_C(2E_{0,z} + E_C)}}, \frac{\sqrt{2}\eta(k_x - ik_y)}{\sqrt{E_C(2E_{0,z} + E_C)}}, \\ &\sqrt{\frac{2E_{0,z} + E_C}{2E_C}}, \frac{i\eta'(k_x + ik_y)}{2E_{g,X}}, -\frac{Pk_x}{E_{g,X}}, -\frac{\Delta_X'}{E_{g,X}}, \\ &-\frac{Pk_y}{E_{g,X}}, -\frac{i\Delta_X'}{E_{g,X}}\Bigg]^T, \end{aligned} \quad (6)$$

$$\begin{aligned}\langle\mathbf{k}, \Downarrow| \simeq \Bigg[&-\frac{\sqrt{2}\eta(k_x - ik_y)}{\sqrt{E_C(2E_{0,z} + E_C)}}, \frac{\sqrt{2}E_{x,y}}{\sqrt{E_C(2E_{0,z} + E_C)}}, \\ &\frac{-i\eta'(k_x + ik_y)}{2E_{g,X}}, \sqrt{\frac{2E_{0,z} + E_C}{2E_C}}, \frac{\Delta_X'}{E_{g,X}}, \\ &-\frac{Pk_x}{E_{g,X}}, \frac{i\Delta_X'}{E_{g,X}}, -\frac{Pk_y}{E_{g,X}}\Bigg], \end{aligned} \quad (7)$$

where $\Delta_X' = \Delta_X + \alpha|k_z|$, $\eta' = 2i\Delta_X'P/E_{g,X}$, and E_C is the energy spacing between the conduction bands [twice the square root in Eq. (5)]. For later use, we define an important parameter $\Delta_C \equiv E_C(\mathbf{k}_0) \simeq 2\hbar^2k_0^2/m_0 \sim 0.5$ eV, which denotes the energy spacing at the valley center (see Fig. 1). State expressions in the x and y valleys are provided in the Supplemental Materials [24]. We can, however, unify features along all crystallographic axes by defining κ:

$$\kappa \equiv \begin{cases} k_y & \text{if } n = x, \\ ik_x & \text{if } n = y, \\ k_x + ik_y & \text{if } n = z. \end{cases} \quad (8)$$

We first briefly discuss the spin mixing, which is a measure of the total magnitude of spin-down components in a $|\Uparrow\rangle$ state (and vice versa). The spin mixing can reach its maximal value (1/2) along certain directions at the edge of the Brillouin zone where it is given by

$$\beta(k_n=0)=(1+\delta_{n,z})\frac{\Delta_X^2}{E_{g,X}^2}+\frac{1}{2}\frac{|\eta\kappa|^2}{E_{\ell,m}+|\eta|^2(k_\ell^2+k_m^2)}. \quad (9)$$

This result elucidates the nature of the spin hot spot [5,28]. At the vicinity of the valley center, the mixing is of the order of 10^{-6}, and it is given by

$$\beta(k_n\sim k_0)=(1+\delta_{n,z})\left(\frac{\Delta_X+\alpha k_0}{E_{g,X}-\frac{\Delta_C}{4}}\right)^2+\left(\frac{2|\eta\kappa|}{\Delta_C}\right)^2. \quad (10)$$

A powerful application of the theory is in elucidating the spin relaxation mechanisms. We focus on intrinsic or nondegenerate n-type silicon, where spin relaxation is governed by electron-phonon interaction across a wide temperature range [5,23,29]. The relaxation rate is

$$\frac{1}{\tau_{s,\nu}}=\frac{2\pi\hbar}{\varrho N_c}\int d^3\mathbf{k}\,e^{-E_\mathbf{k}/k_BT}\int\frac{d^3\mathbf{k}'}{(2\pi)^3}|M_\nu^{sf}(\mathbf{k},\mathbf{k}')|^2\frac{1}{\Omega_\nu(\mathbf{q})}\times\left[\sum_{\pm}(n_{\nu,\mathbf{q}}+\tfrac{1}{2}\pm\tfrac{1}{2})\delta[E_{\mathbf{k}'}-E_\mathbf{k}\pm\Omega_\nu(\mathbf{q})]\right], \quad (11)$$

where $\varrho=2.33\ \mathrm{g/cm^3}$ is the crystal density and $N_c=(2\pi m_d k_BT/\hbar^2)^{3/2}$ is an effective density constant ($m_d^3=m_0m_t^2$). ν, $\mathbf{q}=\mathbf{k}-\mathbf{k}'$, $\Omega_\nu(\mathbf{q})$, and $n_{\nu,\mathbf{q}}$ denote the phonon mode, wave vector, energy, and Bose-Einstein distribution, respectively. The $+$ $(-)$ refers to phonon emission (absorption) processes. $M_\nu^{sf}(\mathbf{k},\mathbf{k}')=\langle\mathbf{k}',\Downarrow|M_{\nu,\mathbf{q}}|\mathbf{k},\Uparrow\rangle$ is the spin-flip matrix element between electronic states in the lower conduction band. A central point in spin relaxation of silicon is that mechanisms that dominate the momentum relaxation are not identical to those that lead to spin relaxation. In the Supplemental Materials, the Hamiltonian model is used to derive selection rules of various spin relaxation processes [24]. Here we derive explicit electron-phonon interaction forms and their ensuing spin relaxation times.

Intravalley scattering.—Inspection of the electronic states reveals that the intraband spin-flip coupling is much smaller than the interband coupling between conduction bands. For example, at the valley center region [$2E_{0,z}\rightarrow E_C$ in Eqs. (6) and (7)], the product square amplitude of the dominant $X_1^1\uparrow$ coefficient in $|\mathbf{k},\Uparrow\rangle$ with the $X_1^1\uparrow$ coefficient in $\langle\mathbf{k}',\Downarrow|$ is smaller than with the $X_1^{2'}\uparrow$ coefficient in $\langle\mathbf{k}',\Downarrow|$ by a factor of $(\Delta_C/E_{g,X})^2\simeq 1/64$. Interband coupling between X_1^1 and $X_1^{2'}$ states is feasible, for example, via the deformation potential Ξ_i, associated with the off-diagonal strain component ($e_{\ell m}$, where n is the valley axis) [11]. The symmetries of this coupling result in a dominant role of the transverse acoustic (TA) phonon mode [24], and the spin-flip matrix element reads

$$|M_{\mathrm{TA}}^{sf}(\mathbf{k},\mathbf{k}')|_{n,n}=\frac{|\eta(\kappa-\kappa')|}{\Delta_c}|\mathbf{k}-\mathbf{k}'|\Xi_i. \quad (12)$$

Intravalley momentum scattering, on the other hand, is governed by the intraband dilation and uniaxial deformation potentials (Ξ_d and Ξ_u) that lead to a dominant role of longitudinal acoustic (LA) phonons [30]. In Eq. (12), we have used a single effective deformation potential $\Xi_i\simeq 8$ eV [31], which absorbs the effect of the valleys' ellipsoidal energy dispersion. Substituting Eq. (12) into Eq. (11) and using the long wavelength limit $\Omega_{\mathrm{TA}}(\mathbf{q})=\hbar v_{\mathrm{TA}}q\ll k_BT$, where $v_{\mathrm{TA}}\simeq 5\times10^5$ cm/sec is the TA phonon speed, we get the average intravalley spin relaxation rate

$$\frac{1}{\tau_{s,i}}=\frac{128}{9}\frac{m_t}{m_{cv}}\left(\frac{\Delta_X}{\Delta_C}\right)^2\left(\frac{2m_d}{\pi}\right)^{3/2}\frac{\Xi_i^2(k_BT)^{5/2}}{\hbar^4\varrho v_{\mathrm{TA}}^2E_{g,X}}. \quad (13)$$

The $T^{5/2}$ dependence was predicted by Yafet (see pp. 75–80 in Ref. [23]). However, our theory reveals the correct magnitude and hidden symmetries: coupling between conduction bands, TA mode dominant role, and the involved wave vector components as shown in Eq. (12) via the κ parameter [defined in Eq. (8)] rather than $|\mathbf{k}-\mathbf{k}'|^2$.

Intervalley g-process scattering.—In this umklapp process, a phonon mode with wave vector $\mathbf{q}_g\sim 0.3\times(2\pi/a)\hat{n}$ is needed to scatter electrons between the $(\pm k_0)\hat{n}$ valleys [8]. g-process momentum scattering is dominated by interaction with longitudinal optical phonons [32]. The dominant g-process spin flips, on the other hand, are governed by interaction with acoustic phonons which are forbidden at zero order for momentum scattering [24]. To understand this behavior, we note that replacing $k_n\rightarrow -k_n$ in the Hamiltonian of the $-n$ valley [Eqs. (3) and (4)] leads to an exchange of coefficients between $X_1^1\leftrightarrow X_1^{2'}$ and $X_4^\ell\leftrightarrow X_4^m$ states in Eqs. (6) and (7). As a result, the dominant spin-flip mechanism during a g process is governed by intraband coupling albeit at opposite valleys (i.e., between respective X_1^1 coefficients of $|\mathbf{k},\Uparrow\rangle$ in the n valley and $\langle\mathbf{k}',\Downarrow|$ in the $-n$ valley). The resulting spin-flip matrix element is

$$|M_g^{sf}(\mathbf{k},\mathbf{k}')|_{n,-n}=D_g\frac{|\eta(\kappa+\kappa')|}{\Delta_c}. \quad (14)$$

Note that when $\kappa=-\kappa'$ the matrix element is zero in accord with time reversal symmetry. The large longitudinal component $|\mathbf{k}-\mathbf{k}'|_n\approx 2k_0$ relates to the dilation and uniaxial deformation potential constants via $D_g\approx 2k_0(\Xi_d+\Xi_u)\approx 4$ eV/Å. As mentioned, this coupling is associated with LA phonon modes where $\Omega_g=\Omega_{\mathrm{LA}}(\mathbf{q}=2k_0\hat{n})\approx 21$ meV. Substituting Eq. (14) into Eq. (11), we get the average g-process spin relaxation rate

$$\frac{1}{\tau_{s,g}}=\frac{32}{9}\frac{m_t}{m_{cv}}\left(\frac{\Delta_X}{\Delta_C}\right)^2\left(\frac{2m_d}{\pi}\right)^{3/2}\frac{\sqrt{\Omega_g}D_g^2}{\hbar^2\varrho E_{g,X}}\cdot\frac{g(y)}{\exp(y)-1}, \quad (15)$$

where $y=\Omega_g/k_BT$ and $g(y)$ is associated with the modified Bessel function of the second kind via:

$$g(y) = \frac{\sqrt{y}}{2}\exp\left(\frac{y}{2}\right)K_2\left(\frac{y}{2}\right) \approx 1 + 5y^{-3/2}. \quad (16)$$

Intervalley f-process scattering.—In this umklapp process, a phonon mode with wave vector $\mathbf{q}_f \approx k_0\hat{n} + k_0\hat{\ell} + (2\pi/a)\hat{m}$ is needed to scatter electrons between valleys that reside in the $\hat{n}$ and $\hat{\ell}$ directions [8]. This wave vector resides on the Σ axis, where spin (momentum) scattering is dominated by phonon modes with Σ_1 and Σ_3 (Σ_1) symmetries [24]. Spin relaxation is unique since it is carried via coupling of valence and conduction bands. This coupling is a result of the nonorthogonal bases of the n and ℓ valleys that are involved in the transition (i.e., $\langle X^1_{1,n}|X^m_{4,\ell}\rangle \neq 0$). The spin-flip matrix element reads

$$|M_f^{sf}(\mathbf{k}, \mathbf{k}')|_{\ell,n} = C_i D_i \frac{\Delta_X + \alpha k_0}{E_{g,X}}. \quad (17)$$

$C_1 = 2$ and $C_3 = 1$ if one of the involved valleys (n or ℓ) is collinear with the spin quantization axis (z) or $C_1 = 0$ and $C_3 = \sqrt{2}$ if both valleys are perpendicular to it [24]. D_i is a scattering constant associated with a phonon mode of Σ_i symmetry in an f process. By using an empirical pseudopotential model, an adiabatic bond-charge model, and a rigid-ion approximation (similar to the procedure in Ref. [5]), the calculated values are $D_1 \approx 12$ eV/Å and $D_3 \approx 5$ eV/Å. The $\Sigma_{1(3)}$ symmetry is governed by the upper (middle) acoustic branch with a phonon energy of $\Omega_{f,1} \approx 47$ meV ($\Omega_{f,3} \approx 23$ meV). Using Eq. (17) and the possibility of scattering to 4 valleys, we get the average f-process spin relaxation rate

$$\frac{1}{\tau_{s,f}} = \frac{16}{3}\left(\frac{\Delta'_X(k_0)}{E_{g,X}}\right)^2\left(\frac{2m_d}{\pi}\right)^{3/2}\sum_{i=1,3}\frac{A_i D_i^2}{\hbar^2\varrho\sqrt{\Omega_{f,i}}}\frac{f(y_i)}{\exp(y_i)-1}, \quad (18)$$

where $\Delta'_X(k_0) = \Delta_X + \alpha k_0$, $A_1 = 2$, $A_3 = 1$, and $y_i = \Omega_{f,i}/k_B T$. $f(y) = \sqrt{y}\exp(y/2)K_{-1}(y/2)$ is associated with the modified Bessel function of the second kind [$\sqrt{\pi} \lesssim f(y_i) \lesssim 3$ when $10\ \mathrm{K} < T < 400\ \mathrm{K}$]. Figure 1(b) shows the spin relaxation of all mentioned processes as a function of temperature. Spin relaxation is dominated by intravalley (f-process) scattering in low (high) temperatures. The figure shows excellent agreement with experimental results which have used electron spin resonance ("×" symbols at $T > 150$ K) [20,21] and spin transport via a Larmor-clock analysis [33] and spin-valve magnetoresistance [34].

In conclusion, we have derived a Hamiltonian that elucidates the spin properties of conduction electrons in silicon. Applications of the Hamiltonian were used to extract analytical spin relaxation times and to explain the electron-phonon mechanisms that dictate the relaxation. The theory also establishes a solid ground to analytically study spin relaxation in doped silicon via scattering with impurities or via exchange with holes. In addition, straightforward extensions can be made to describe stressed silicon (incorporating strain-invariant parameters) or to study spin properties in silicon heterostructures and nanostructures by plane wave expansions. Finally, the theory guides experimental studies of spin properties by providing lucid insights into the various scattering mechanisms. New experiments can be designed to extract the spin-orbit coupling parameters (Δ_X and α). These parameters can then be used in the modeling of spintronic devices [35,36].

This work is supported by AFOSR Contract No. FA9550-09-1-0493 and by NSF Contract No. ECCS-0824075. We deeply thank Mr. Y. Song for providing elaborate numerical results which served as a crucial reference for our analytical results.

*pengke@ece.rochester.edu

[1] I. Appelbaum, B. Q. Huang, and D. J. Monsma, Nature (London) **447**, 295 (2007).
[2] B. T. Jonker, G. Kioseoglou, A. T. Hanbicki, C. H. Li, and P. E. Thompson, Nature Phys. **3**, 542 (2007).
[3] S. P. Dash, S. Sharma, R. S. Patel, M. P. de Jong, and R. Jansen, Nature (London) **462**, 491 (2009).
[4] T. Suzuki, T. Sasaki, T. Oikawa, M. Shiraishi, Y. Suzuki, and K. Noguchi, Appl. Phys. Express **4**, 023003 (2011).
[5] J. L. Cheng, M. W. Wu, and J. Fabian, Phys. Rev. Lett. **104**, 016601 (2010).
[6] I. Žutić, J. Fabian, and S. Das Sarma, Rev. Mod. Phys. **76**, 323 (2004).
[7] H. Jones, *Theory of Brillouin Zones and Electronic States in Crystals* (North-Holland, Amsterdam, 1960), p. 15.
[8] P. Y. Yu and M. Cardona, *Fundamentals of Semiconductors* (Springer, Berlin, 2005), 3rd ed., Chaps. 2–5.
[9] J. M. Luttinger and W. Kohn, Phys. Rev. **97**, 869 (1955).
[10] E. O. Kane, J. Phys. Chem. Solids **1**, 249 (1957).
[11] J. C. Hensel, H. Hasegawa, and M. Nakayama, Phys. Rev. **138**, A225 (1965).
[12] M. Cardona and F. H. Pollak, Phys. Rev. **142**, 530 (1966).
[13] G. Dresselhaus and M. S. Dresselhaus, Phys. Rev. **160**, 649 (1967).
[14] G. L. Bir and G. E. Pikus, *Symmetry and Strain-Induced Effects in Semiconductors* (Halsted, Jerusalem, 1974), Chaps. 3 and 4.
[15] E. L. Ivchenko and G. E. Pikus, *Superlattices and Other Heterostrucrures* (Springer, Heidelberg, 1995).
[16] J.-M. Jancu, R. Scholz, F. Beltram, and F. Bassani, Phys. Rev. B **57**, 6493 (1998).
[17] R. Winkler, *Spin-Orbit Coupling Effects in Two-Dimensional Electron and Hole Systems* (Springer, Berlin, 2003), Appendix B.
[18] A. Honig and J. Combrisson, Phys. Rev. **102**, 917 (1956).
[19] G. Feher, Phys. Rev. **114**, 1219 (1959).
[20] G. Lancaster, J. A. Van Wyk, and E. E. Schneider, Proc. Phys. Soc. London **84**, 19 (1964).
[21] D. J. Lépine, Phys. Rev. B **2**, 2429 (1970).
[22] V. Zarifis and T. G. Castner, Phys. Rev. B **36**, 6198 (1987).

[23] Y. Yafet, in *Solid State Physics*, edited by F. Seitz and D. Turnbull (Academic, New York, 1963), Vol. 14, p. 1.
[24] See Supplemental Material at http://link.aps.org/supplemental/10.1103/PhysRevLett.107.107203 for technical details of the space group, of the form of H_{vv} and detailed energy dispersions, of the 8-component states in the x and y valleys, and of selection rules.
[25] The two-band degeneracies result from time reversal and glide reflection symmetries.
[26] P.-O. Löwdin, J. Chem. Phys. **19**, 1396 (1951).
[27] J. R. Chelikowsky and M. L. Cohen, Phys. Rev. B **14**, 556 (1976).
[28] J. Fabian and S. Das Sarma, Phys. Rev. Lett. **81**, 5624 (1998).
[29] R. J. Elliott, Phys. Rev. **96**, 266 (1954).
[30] C. Herring and E. Vogt, Phys. Rev. **101**, 944 (1956).
[31] L. D. Laude, F. H. Pollak, and M. Cardona, Phys. Rev. B **3**, 2623 (1971).
[32] H. W. Streitwolf, Phys. Status Solidi **37**, K47 (1970).
[33] H.-J. Jang and I. Appelbaum, Phys. Rev. Lett. **103**, 117202 (2009); B. Huang and I. Appelbaum, Phys. Rev. B **82**, 241202(R) (2010).
[34] Ian Appelbaum (private communication).
[35] I. Žutić, J. Fabian, and S. C. Erwin, Phys. Rev. Lett. **97**, 026602 (2006).
[36] H. Dery, P. Dalal, Ł Cywiński, and L. J. Sham, Nature (London) **447**, 573 (2007).